Received: 15 August 2024 | Revised: 24 November 2024 | Accepted: 04 January 2025

DOI: 10.5185/amlett.2025.011771

OPEN ACCESS

RESEARCH

Green Synthesis of Gold Nanoparticles using Aloe Vera Leaf Extracts and its Antibacterial Activity

Ryan M. Lumod[1]*, Khia Jane D. Avila[1], Rolen Brian P. Rivera[1,2], Miceh Rose A. Magdadar[2,6], Noel Lito B. Sayson[1,2], Felmer S. Latayada[3], Gerard G. Dumancas[4], Rey Y. Capangpangan[5], Arnold C. Alguno[1]

[1]Research Center for Energy Efficient Materials (RCEEM), Premier Research Institute of Science and Mathematics (PRISM), Mindanao State University – Iligan Institute of Technology, A. Bonifacio Avenue, Iligan City, 9200 Philippines

[2]Department of Physics, Mindanao State University – Iligan Institute of Technology, A. Bonifacio Avenue, Iligan City, 9200 Philippines

[3]Department of Chemistry, Caraga State University, Butuan City 8600, Philippines

[4]Department of Chemistry, New Science Building, North Carolina Agricultural and Technical State University 1601 E. Market Street, Greensboro, NC 27411 USA

[5]Department. of Physical Science & Mathematics, Mindanao State University at Naawan, Naawan Misamis Oriental, 9023 Philippines

[6]Mindanao State University, Lanao del Norte Agricultural College, Lanao del Norte, Philippines

***Corresponding author:**
E-mail: ryan.lumod@g.msuiit.edu.ph

ABSTRACT

Gold nanoparticles (AuNPs) have wide-ranging applications across scientific disciplines and industries. However, its conventional synthesis methods pose environmental and health risks, prompting the rise of green chemistry for sustainable and eco-friendly nanoparticle production. Plant extracts rich in bioactive compounds capable of reducing and capping nanoparticles have emerged as promising alternatives. Among these sources, Aloe vera, renowned for its diverse phytochemicals, presents an attractive avenue for nanoparticle synthesis devoid of hazardous reagents. This study delves into the one-step green synthesis of AuNPs employing aloe vera extract and examines their antibacterial efficacy against Gram-positive and Gram-negative bacteria. The synthesized AuNPs exhibited a reddish-purple color with localized surface plasmon resonance peaks at 529 nm, 535 nm, and 541 nm, corresponding to varying gold precursor concentrations (0.1 mM, 0.3 mM, and 0.5 mM). FTIR analysis confirmed the presence of bioactive compounds involved in the reduction and capping of AuNPs. Characterization via Transmission Electron Microscopy showed spherical AuNPs ranging from 10 nm to 39 nm in diameter, with stability indicated by zeta potential values of -37.3 mV, -28.7 mV, and -24.7 mV for the respective concentrations. Notably, AV-AuNPs demonstrated significant antibacterial activity, with inhibition zones of 34 mm against E. coli and 18 mm against B. subtilis, attributed to their ability to penetrate bacterial membranes and induce cell lysis.

KEYWORDS

Green Synthesis, Gold Nanoparticle, Aloe vera, Antibacterial Activity, size variation.

INTRODUCTION

In recent years, there has been a significant surge in the synthesis and utilization of nanomaterials across diverse sectors encompassing catalysis, electronics, biomedical engineering, energy science, and optics [**1–3**]. Noble metal nanoparticles, including gold, silver, zinc oxides, and platinum, find extensive applications in medical, pharmaceutical, and consumer domains due to their distinctive surface energy, surface-to-volume ratio, and other inherent properties they possess [**4–6**].

Gold nanoparticles (AuNPs) stand out among metallic nanoparticles due to their unique physical and chemical properties, attracting significant attention for their diverse applications in biomedicine, particularly in combating antibiotic-resistant bacteria [**7–10**]. The escalating challenge of antibiotic resistance has spurred the quest for alternative antibacterial solutions. Prior research underscores the strong antibacterial effectiveness of AuNPs, which operate through various mechanisms. One primary mode is their interaction with bacterial cell membranes, resulting in cell death. Moreover, their large surface area enables interactions with cellular components,

disrupting their functions and inhibiting bacterial proliferation [**11–14**].

Various physical and chemical methodologies have been devised to synthesize gold nanoparticles [**15,16**]. However, conventional protocols associated with these methods involve using toxic chemicals and high temperatures during synthesis, which poses risks to human health and the environment [**17**]. Consequently, there is a growing emphasis on green chemistry principles, which advocate for sustainable approaches to chemical processes, including the synthesis of nanoparticles [**18–21**].

Natural sources, particularly plant extracts abundant in bioactive compounds with nanoparticle-reducing and capping capabilities, have emerged as promising alternatives [**21–25**]. Plant extracts are highly preferred for AuNP synthesis due to their eco-friendly nature, cost-effectiveness, and lower toxicity than alternative synthetic methods. Thus far, various plant extracts have been documented for their successful involvement in synthesizing AuNPs with antibacterial properties. These include *Terminalia arjuna*, [**26**] Jack fruit, [**27**] *Ziziphus zizyphus*, [**28**] *Mammea suriga*, [**29**] *Xanthium strumarium*, [**30**] *Rauwolfia serpentina*, [**31**] *Mentha spicata*, [**32**] and *Vitex negundo* [**33**].

Among these sources, Aloe barbadensis miller, known as Aloe vera, is renowned for its diverse phytochemicals and presents an attractive avenue for nanoparticle synthesis devoid of hazardous reagents [**34**]. Aloe vera is a succulent plant widely used for its medicinal properties. Originally from Africa, it is now grown in various parts of the world, including the Philippines. Aloe vera has been used for decades to treat multiple health conditions, including skin infections, burns, and wounds. In recent years, there has been a growing interest in the antibacterial properties of Aloe vera. This plant contains several effective compounds against bacteria, including anthraquinones like aloin and emodin, polysaccharides, and lectins [**35–37**].

Previous studies have identified the presence of polysaccharides, phenolic acids, and other biomolecules in aloe vera extract, endowing it with potent reducing and stabilizing properties conducive to nanoparticle synthesis, including AgNPs, [**38**] CuO, [**39**] and AuNPs [**40,41**]. Aloe vera is chosen as the reducing and stabilizing agent for AuNP synthesis because of its abundance and readily available nature, making it a cost-effective option. However, high precursor concentrations were employed in this literature, and no further investigations were conducted in utilizing lower precursor concentrations, which could be more economical and resource-efficient.

This study explores the potential of aloe vera extracts for efficiently reducing gold ions at low precursor concentrations, leading to well-defined AuNPs of varied sizes through a straightforward and facile process. Further, this study investigates the impact of varying AuNP sizes synthesized using Aloe vera extract to determine the optimal size range for maximizing their antibacterial potential against both gram-positive and gram-negative bacteria. The resultant AuNPs underwent comprehensive characterization utilizing transmission electron microscopy (TEM), UV-vis spectroscopy, Fourier transform infrared spectroscopy (FTIR), and dynamic light scattering (DLS). The gold nanoparticles' antibacterial efficacy against gram-negative (*E. coli*) and gram-positive bacteria (*B. subtilis*) was systematically examined.

EXPERIMENTAL

Materials

Aloe vera leaves were obtained from a local market in General Santos City, Philippines. Gold (III) chloride hydrate ($HAuCl_4$) (99.995% trace metals basis, analytical grade) was purchased from Sigma-Aldrich (Germany). Ethanol (EMSURE, ACS reagent) was acquired from Merck KGaA (Germany). Milli-Q ultrapure water (18.2 MΩ.cm-1) was used as a synthesis solvent from Merck KGaA in Germany.

Preparation of Aloe vera leaf extract

Aloe vera leaves were chosen because of their medicinal properties and natural abundance. The acquired aloe vera leaves underwent meticulous washing with tap water, followed by two rinses with Milli-Q ultrapure water to eliminate impurities. Subsequently, the leaves were sectioned into small segments and subjected to overnight drying at 60°C in an oven. Once desiccated, the aloe vera leaves were finely pulverized using a stainless-steel mixer. The resulting aloe vera powder (10g) was subjected to maceration in 100 mL of ethanol for 72 hours with periodic agitation. Following maceration, the mixture underwent dual filtration using a Whatman No. 1 filter paper, followed by heating and stirring for one hour at 60°C to remove residual ethanol. The resultant blend was allowed to cool and stored at 4ºC in a refrigerator for subsequent use in gold nanoparticle synthesis. This resulting extract served as the aloe vera (AV) solution for further experimentation.

Synthesis of Aloe vera-mediated gold nanoparticles (AV-AuNPs)

To synthesize AV-AuNPs, a 50 mL aqueous solution of $HAuCl_4$ was introduced into an Erlenmeyer flask and heated to 60 ºC under stirring in a water bath. Upon reaching the designated temperature, 5 mL of aloe vera extract was promptly introduced into the $HAuCl_4$ solution. This resulted in a gradual transition in the solution's color from pale yellow to purple-red, indicating successful AuNP formation. The influence of a reduced precursor concentration on AuNP morphology was investigated by modulating the molar concentration of the $HAuCl_4$ solution from 0.1 mM to 0.5 mM while maintaining a constant volume of aloe vera extract. Subsequently, the solution was allowed to cool to room temperature before undergoing various characterization techniques. All experiments were conducted in triplicate for statistical rigor.

Characterization of AV-AuNPs

The synthesized AV-AuNPs' ultraviolet-visible spectra were acquired using a Thermo-Scientific GENESYS 10S (Massachusetts, USA) spectrophotometer. The samples were scanned over the 200 to 1000 nm spectral range with a spectral resolution of 1.8 nm.

Hydrodynamic particle size and zeta potential measurements of the colloidal AV-AuNPs were carried out using a Nanotrac Wave II Analyzer Zeta (Pennsylvania, USA). A 1 mL colloidal solution of each synthesized AV-AuNP was placed in a fixed sample holder and allowed to run for 1 minute. All measurements were conducted at room temperature.

Fourier transform infrared spectroscopy (FTIR) was also utilized to distinguish the chemical bonds on the synthesized AV-AuNPs and Aloe vera extract. Infrared transmittance spectra were recorded using a Shimadzu IR Tracer-100 (Japan) FT-IR spectrometer in the 4000-400 cm^{-1} wavelength range. A 2.0 mL AV-AuNP colloidal solution was placed in an Eppendorf tube and centrifuged at 9000 rpm for 30 mins. Following the removal of the supernatant, a small amount of the sediments was allowed to air-dry on the FTIR sample platform before analysis.

The morphological assessment of the gold nanoparticles was examined using TEM. Micrographs of the samples were obtained using a JEM 2100 Plus LaB6 (Japan) TEM equipped with STEM capabilities with resolutions of up to 0.14nm at 200kV. A Pasteur pipette dispensed adequate AV-AuNP colloidal solution onto a 3mm Cu grid with formvar/carbon supporting film. The solution was then dried for 15 minutes. The Cu grid was mounted on a TEM holder and placed in a dry pump multi-station for 24 hours to outgas before characterization.

Stability of AV-AuNPs solution

Assessing the stability of nanoparticles is crucial when considering their usage in biomedical applications. In this study, we have investigated the stability of as-synthesized AV-AuNPs at different pH levels. The AV-AuNP solution's pH, initially at pH 7, was adjusted to pH levels 4, 6, 8, 10, and 12 using 0.25 M HCl and 0.25 M NaOH. The solutions were then left for 24 hours to incubate. Changes in the UV-Vis spectra were measured to evaluate the stability of the nanoparticles. Moreover, a time-dependent stability test was also conducted. Here, AV-AuNPs were stored at 4ºC at various durations, i.e., 1, 15, and 30 days. Then, 2 mL aliquots were analyzed using UV-vis spectra to evaluate the changes in the SPR peak with increasing storage time.

Antibacterial Activity of AV-AuNP

The Antibacterial activity of Aloe Vera (AV) extracts and AV-AuNPs were tested against gram-negative E. coli (*Escherichia coli*) and gram-positive B. subtilis (*Bacillus subtilis*) bacteria using the disc diffusion method. The organisms were sub-cultured in a nutrient broth overnight at 37°C. Consequently, Nutrient Agar was swabbed with respective subcultures. Discs containing AV, AV-AuNPs, positive control (Amoxicillin), and Negative control (Milli-Q ultrapure water) were then arranged on the swabbed agar surface and incubated at 37°C for 24 h. The results were read by measuring the diameter of the inhibition zone (mm) using a vernier caliper. The test was done in triplicates.

RESULTS AND DISCUSSION

This study reports using a more straightforward and greener method for synthesizing AuNPs using aloe vera leaf extract as the reducing and stabilizing agent. Successful green synthesis of AuNPs was confirmed by the change in color of the mixture from pale yellow to reddish-purple. The color changes are due to the excitation of surface plasmon vibration in gold nanoparticles. **Fig. 1** shows the UV-Vis spectra of AuNPs at various concentrations of $HAuCl_4$. The LSPR of the synthesized AV-AuNPs exhibited singular, well-defined peaks at 529 nm, 535 nm, and 541 nm for 0.1 mM, 0.3 mM, and 0.3 mM, respectively. The observed absorbance profile is attributed to the characteristic LSPR of spherical AuNPs [**42,43**]. Furthermore, the LSPR of AV- AuNPs shifted to a higher wavelength (red-shift) with increasing $HAuCl_4$ concentration. This red shift phenomenon is associated with the plasmonic properties of larger AuNPs. This shift occurs due to the enhanced electron density and plasmon coupling in the larger nanoparticles, leading to higher resonance energy [**44–46**]. Consequently, this phenomenon influences our color perception, resulting in differences in the color of the solutions, as depicted in the inset of **Fig. 1**.

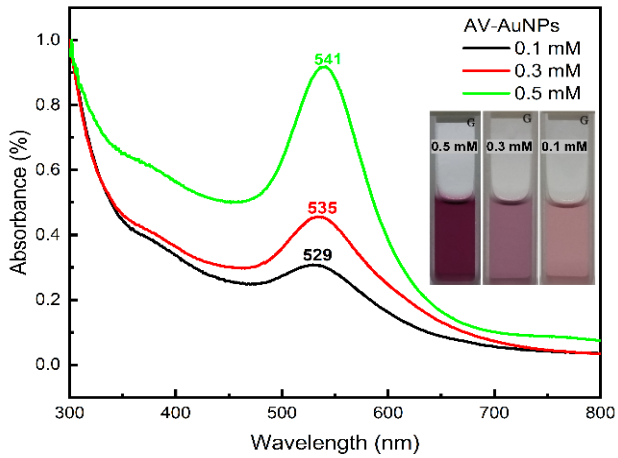

Fig. 1. UV-vis absorbance spectra of AV-AuNPs with varying gold precursor concentrations. The inset displays the actual photographs of AV-AuNPs.

UV-Vis was used to monitor AV-AuNP reaction kinetics over 1 hour at different intervals to understand the particle's growth process. **Fig. 2** shows the UV-vis normalized spectra of AV-AuNPs prepared by using 0.1 mM, 0.3 mM, and 0.5 mM gold precursor concentrations acquired at various time intervals. The insets display the typical change in color of Au colloids from pale yellow to

pink and then reddish-purple as the reaction progresses. The spectra also show an increase in absorbance value with increasing reaction time, which indicates the further reduction of metal ions and an increase in nanoparticle concentration. It is worth noting that as the concentration of the gold precursor increases, the synthesis time for AuNPs decreases.

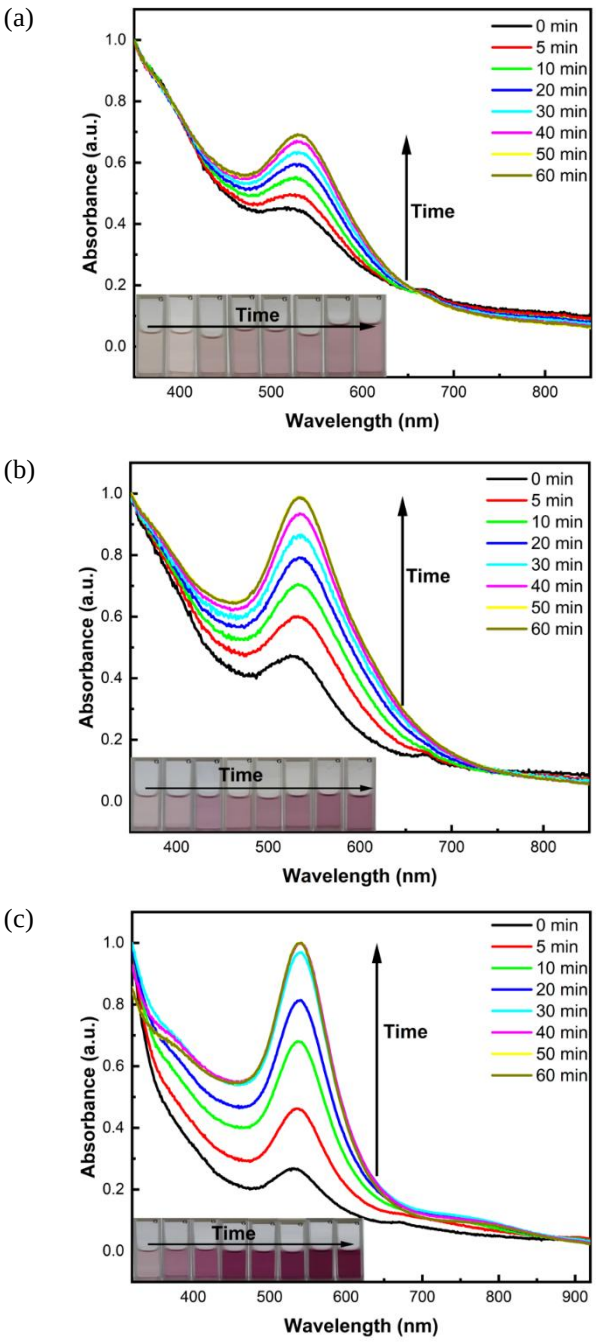

Fig. 2. UV-vis absorption spectra for the continuous growth of AV-AuNPs. Prepared by using (a) 0.1 mM, (S2) 0.5 mM, and (c) 0.5 mM gold precursor concentration. Experiments were performed at 60°C. The insets display the actual photographs of the AV-AuNP's growth within 1 h with different time intervals.

The intensity at 541 nm for 0.5 mM AV-AuNPs increases with time and reaches a constant value after 40 minutes, while the intensity at 535 nm for 0.3 mM AV-AuNPs reaches a steady value after approximately 50 minutes, similar to 0.1 mM AV-AuNPs with intensity at 529 nm. In general, a higher concentration of gold precursor results in a higher rate of formation of the nucleation center and an increased rate of nanoparticle growth, which induces the overall time required for the synthesis. After one hour of further reaction, the spectrum had no significant change. The final absorbance value and peak wavelength position remained constant after one month of storage.

The average size and the surface morphology of the prepared AV-AuNPs were determined using TEM. As projected by the UV-vis spectra, the TEM micrographs presented in **Fig. 3** confirm the presence of spherical gold nanoparticles. Consequently, based on the obtained histograms, the mean particle diameter was determined to be 10.19 ± 3.22 nm, 29.08 ± 2.8 nm, and 37.91 ± 4.42 nm for AV-AuNPs prepared with 0.1 mM, 0.3 mM, and 0.5 mM precursor concentration, respectively. Remarkably, triangular and hexagonal shapes were also present on the synthesized AV-AuNPs. Various shapes were observed due to the complex components in the aloe vera extract that have different reducing capabilities.

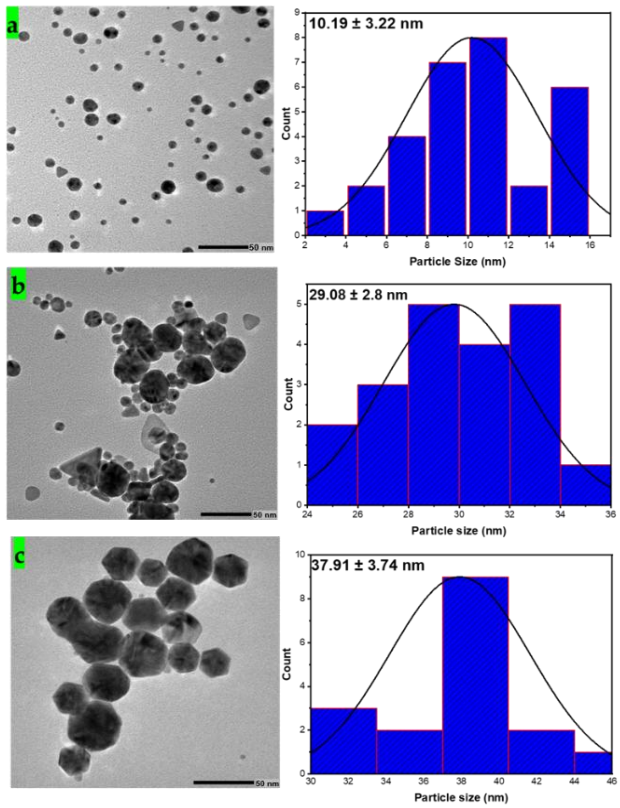

Fig. 3. (Left) TEM micrographs of AV-AuNPs at 50 nm scale prepared with (a) 0.1 mM, (b) 0.3 mM, and (c) 0.1 mM gold precursor. The shape of most NPs is spherical, while triangular and hexagonal shapes are also observed. (Right) Corresponding histogram of the particle size distribution.

Distributions of the hydrodynamic particle size of the AV-AuNPs in different $HAuCl_4$ concentrations were measured by DLS measurements to validate the nanoparticle size obtained from TEM. The results are presented in **Fig. 4**, where scattering distribution is shown as a function of the logarithm of the particle diameter. It is important to note that the hydrodynamic particle size refers to the effective size of the particle, taking into account its interactions with the surrounding solvent or medium, and it includes the size of the nanoparticle core as well as any stabilizing layers or compounds from the aloe vera extracts attached to its surface [**47**].

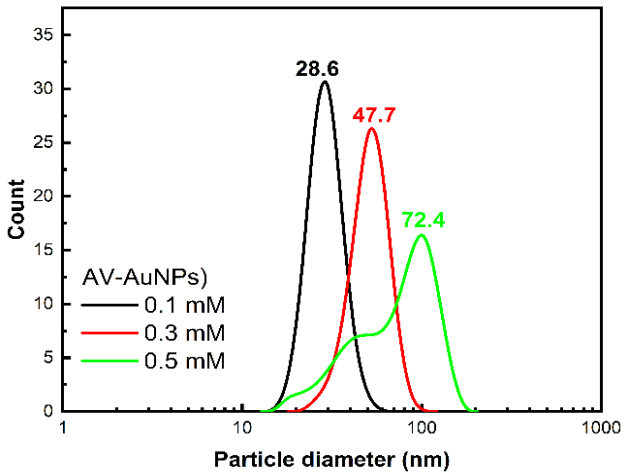

Fig. 4. Size distribution of AV-AuNPs with varying concentrations of gold precursor concentration. The increase in precursor concentration increased the hydrodynamic sizes of nanoparticles.

The hydrodynamic diameter of AV-AuNPs colloidal solution increases from 28.6 nm for 0.1 mM AV-AuNPs to 72.4 nm for 0.5 mM Av-AuNPs. This increase in the hydrodynamic diameter is a consequence of the increasing concentration of $HAuCl_4$. When the concentration of the gold precursor is raised, more gold atoms are available for nucleation and growth, forming larger nanoparticles. As a result, higher precursor concentrations often increase the average size of nanoparticles, including their hydrodynamic size. Zeta potential measurements were used to assess the stability of the nanoparticles. Previous research suggests that a zeta potential value ranging from -25 mV to +25 mV indicates higher stability. A more negative or positive zeta potential helps to repel the particles from each other, thus enhancing their stability [**48**]. The AV-AuNP colloidal solutions with $HAuCl_4$ concentrations of 0.1 mM, 0.3 mM, and 0.5 mM showed zeta potentials of -37.3 mV, -28.7 mV, and -24.7 mV, respectively, falling within the optimal range for stability. This indicates that they possess good stability. Aloe vera contains natural stabilizing agents like polysaccharides and proteins, which can adhere to the AuNP surface, forming a stabilizing layer. This layer contributes to the negative zeta potential by exposing negatively charged groups to the surrounding medium.

FTIR analysis was conducted to determine the chemical composition of the Aloe vera extract and the synthesized AV-AuNPS. **Fig. 5** shows the FTIR spectra of the Aloe vera gel extract and Aloe vera-mediated gold nanoparticles (AV-AuNPs) at different $HAuCl_4$ concentrations.

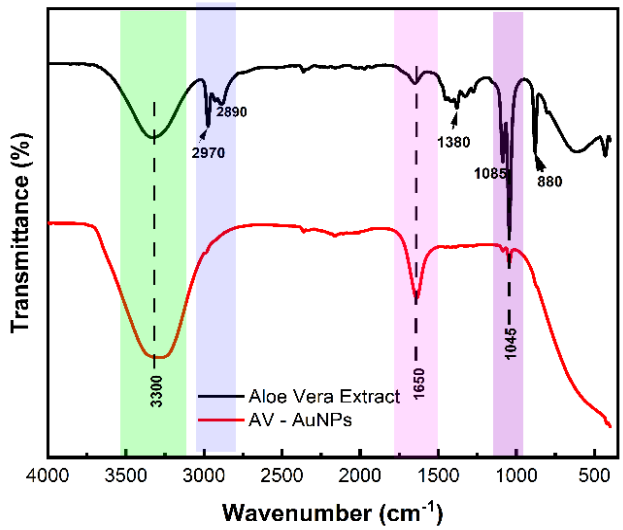

Fig. 5. FTIR spectra of Aloe vera extract (black line) and AV-AuNPs (red line).

Aloe vera extracts contain various compounds that can be analyzed using FTIR spectroscopy. FTIR measures the absorption of infrared light by different chemical functional groups in the sample. The broad spectra at 3600 cm^{-1} to 3100 cm^{-1} correspond to the stretching mode of vibration of the hydroxyl (OH) groups of alcohol or phenolic compounds. The peak at 2975 cm^{-1} is attributed to the C-H stretching of aliphatic hydrocarbons. In the extract, this peak may indicate the presence of fatty acids or other aliphatic compounds. A faint peak at 1650 cm^{-1} corresponds to the carbonyl (C=O) groups. This suggests that the extract contains compounds with carbonyl groups, such as Amino acids and acetylated polysaccharides. The peak at 1045 cm^{-1} is attributed to the stretching vibration of the C-O bond. This also confirms the presence of polysaccharides, such as acemannan, which are significant components of aloe vera leaves [**38,49,50**].

When aloe vera extract is used as a reducing agent for gold nanoparticle synthesis, it can potentially lead to changes in the FTIR peaks observed compared to the original extract. Reducing gold ions to form gold nanoparticles involves chemical interactions between the extract's constituents and the gold ions, which can alter the extract's functional groups and overall composition. The slight disappearance of 1045 cm^{-1} can be attributed to the interaction of acemannan in the reduction process of gold ions. Thus, the frequency of the C-O stretching vibrations was altered. The formation of gold nanoparticles leads to an intense form of peaks at 1650 cm^{-1}, attributed to the C=O bonds, which indicates that amino acids are also present on

the surface of AV-AuNPs. Much broader O-H spectra at 3000 cm^{-1} to 3600 cm^{-1} were also observed. This is attributed to the interaction of phenolic compounds, including flavonoids, with the gold ions during the reduction process [**51,52**].

The assessment of nanoparticle stability across a diverse range of pH levels is imperative when considering their application in biological or medical contexts, as these often involve buffering solutions. In this study, the stability of the as-synthesized AV-AuNPs was scrutinized under various pH conditions by adjusting its pH values using 0.25M NaOH and HCl, spanning from pH 4 to pH 12, for 24 hours. Subsequently, UV-vis absorption spectra were monitored. As illustrated in **Fig. 6** (Left), no significant alterations in absorption spectra were discernible for at least 24 hours, indicating robust stability of the resultant AV-AuNPs across a spectrum of pH conditions. Further, the time-dependence stability of AV-AuNPs stored at 4°C under various durations was also investigated to demonstrate the colloidal stability of AV-AuNPs. It can be observed in **Fig. 6** (Right) that there are no distinct changes in the absorption spectra of the nanoparticle with increasing storage time. In addition, the color of the AV-AuNP solutions remained unchanged even after 30 days of storage at 4°C, indicating the colloidal stability of the solution (see inset **Fig. 6** (Right).

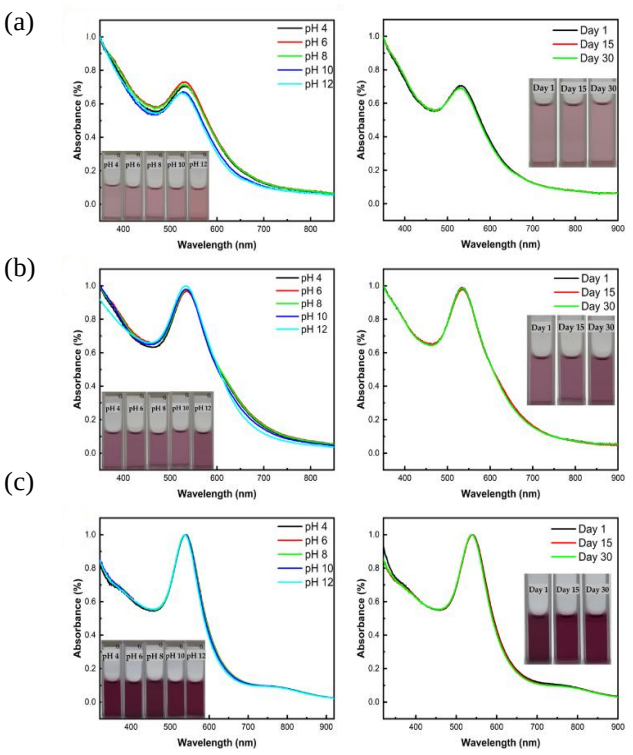

Fig. 6. (Left) UV-vis spectra of AV-AuNPs solutions recorded at 24 h with different pH values. (Right) Time-dependence stability study of AV-AuNPs stored at 4°C for various durations. (a) 0.1 mM AV-AuNPs; (b) 0.3 mM AV-AuNPs; and (c) 0.5 mM AV-AuNPs. All samples are stable across varied pH conditions and storage durations. The inset displays the actual appearance of AV-AuNP solutions.

The stability exhibited by AuNPs under diverse pH conditions and long storage durations facilitated by aloe vera can be attributed to the diverse phytochemicals present in the extracts. Certain compounds, such as polyphenols, flavonoids, alkaloids, terpenoids, and proteins inherent in aloe vera, have been identified as potential contributors to the stability of AuNPs. These compounds can serve as reducing and capping agents during nanoparticle synthesis, thereby furnishing stability across varied pH environments [**35,37,49**].

Gold nanoparticles have been shown to exhibit superior antibacterial activity compared to other metallic nanoparticles [**12,14,53**]. AV-AuNPs were studied for their antibacterial activity against gram-negative E. coli and gram-positive B. subtilis bacteria to demonstrate this activity.

The disc diffusion method was employed to assess the antibacterial activity of AV, AV-AuNPs, and the positive control (amoxicillin) on nutrient agar with a disc diameter of 6 mm. To probe the impact of nanoparticle size on bacterial inhibition zones, a fixed concentration of 200 µg/ml was utilized for samples 0.5 mM (S1), 0.3 mM (S2), and 0.1 mM (S3) AV-AuNPs, with the positive control's concentration held constant at the same level.

Aloe vera has been documented to possess notable antibacterial properties [**36,37**]. The plant harbors various compounds, including anthraquinones, polysaccharides, and lectins, demonstrating inhibitory effects against a broad spectrum of bacteria [**35,54**]. Additionally, it has been reported that AuNPs release Au+ ions, contributing to the antibacterial activity of AV-AuNPs [**53**]. The substantial antibacterial efficacy of AV-AuNPs, as depicted in **Fig. 7**, is likely attributed to the synergistic antibacterial effects of AuNPs and the bioactive compounds present in aloe vera.

Observations from **Fig. 7** and **Table 1** revealed that all AV-AuNP samples of varying particle sizes exhibited notable inhibition zones of 31.5 ± 2.1 mm, 32.5 ± 1.4 mm, and 33.75 ± 1.3 mm for S1, S2, and S3, respectively, against gram-negative E. coli bacteria. These findings align with the inhibition zone obtained from the positive control, amoxicillin (ZOI = 34.0 ± 0 mm). The aloe vera extract also displayed an inhibition zone of 12.8 ± 2.2 mm.

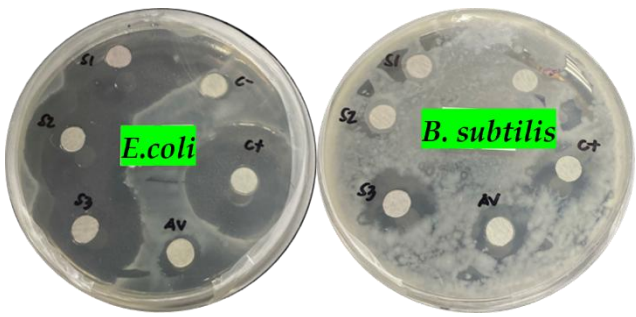

Fig. 7. Antibacterial Activity of aloe vera-mediated gold nanoparticles against E. coli and B. subtilis using disc diffusion method. (S1) 0.5 mM AV-AuNPs; (S2) 0.3 mM AV-AuNPs; and (S3) 0.1 mM AV-AuNPs, (AV) Aloe vera extract, (C+) Amoxicillin, and (C-) Water.

Conversely, no inhibition zones were observed for the larger AV-AuNP samples against the gram-positive bacteria *B. subtilis*. However, the S3 sample exhibited an inhibition zone of 17.25 ± 1.5 mm, similar to the positive control with an 18.0 ± 1.2 mm inhibition zone. The aloe vera extract also demonstrated inhibitory activity against gram-positive bacteria, yielding an inhibition zone of 10.75 ± 2.5 mm.

Table 1. Zone of Inhibition measurement of Aloe vera (AV) and AV-AuNPs.

		Zone of Inhibition (mm)	
AV-AuNPs	**TEM Particle Size**	**E. coli**	**B. subtilis**
0.5 mM	37.91 ± 4.42	31.5 ± 2.1	0
0.3 mM	29.08 ± 2.8	32.5 ± 1.4	0
0.1 mM	10.19 ± 3.22	33.75 ± 1.3	33.75 ± 1.3
AV extract	-	12.8 ± 2.2	10.75 ± 2.5
Positive control	-	34.0 ± 0	18.0 ± 1.2
Negative control	-	0	0

The data highlights a significant disparity in the diameter of the inhibition zone between gram-negative and gram-positive bacteria, a distinction likely rooted in variances in their respective cell wall structures and the dimensions of the nanoparticles [**55,56**]. Gram-positive bacteria, typified by B. subtilis, are characterized by a robust peptidoglycan layer that affords considerable protection against antibacterial agents [**57,58**]. The reduced size of AV-AuNPs translates to an augmented surface area to volume ratio, facilitating enhanced interaction and potential permeation of this protective layer. Conversely, larger AV-AuNPs, with their relatively diminished surface area to volume ratio, may encounter challenges in breaching the dense peptidoglycan layer, impeding access to the inner membrane and cellular constituents [**59,60**].

In contrast, gram-negative bacteria such as *E. coli* feature thinner peptidoglycan layers and outer membranes [**33**], rendering them more susceptible to membrane disruption and subsequent cellular demise. The architectural characteristics of gram-negative bacteria render them more permeable to the AV-AuNPs, facilitating their penetration through the cell wall and culminating in cell death However, ongoing investigations into AV-AuNPs and their antibacterial modalities underscore the imperative for further inquiry. Although gram-negative bacteria generally exhibit heightened susceptibility, the precise factors and underlying mechanisms remain intricate and warrant continued exploration. **Fig. 8** shows the proposed schematic antibacterial activity of AV-AuNPs against E. coli and B. subtilis.

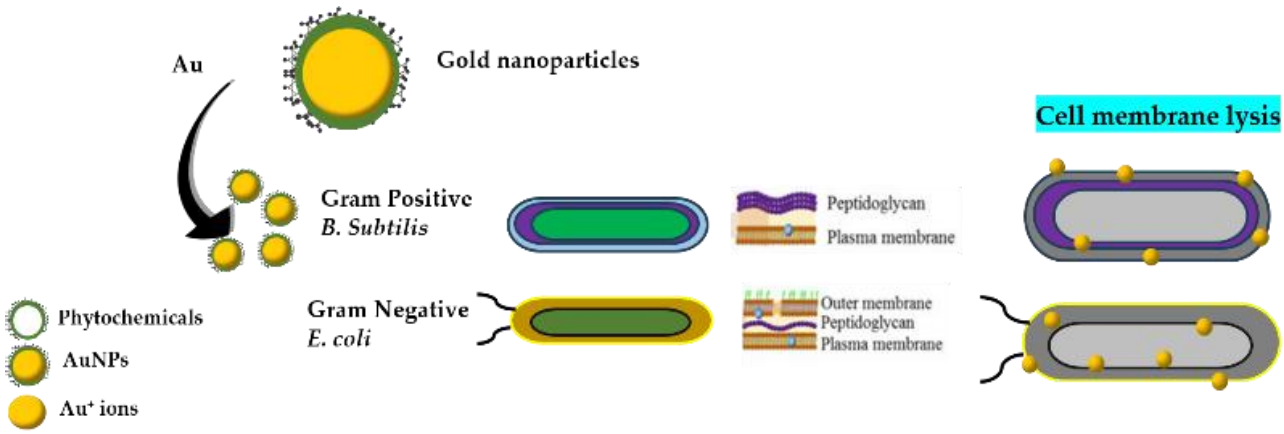

Fig. 8. Antibacterial Activity of aloe vera-mediated gold nanoparticles against E. coli and B. subtilis

CONCLUSION

The present study highlights the efficacy of aloe vera leaf extracts as effective and environmentally sustainable agents for the green synthesis of gold nanoparticles (AuNPs). The resulting AV-AuNPs, characterized by average particle sizes of 37.91 ± 4.42 nm, 29.08 ± 2.8 nm, and 10.19 ± 3.22 nm, were tailored by modulating the concentration of the gold precursor solution. FTIR spectra analysis confirmed the pivotal role of Aloe vera biomolecules, encompassing phenolic compounds, flavonoids, and acetylated polysaccharides, in reducing and encapsulating AuNPs.

Notably, the AV-AuNPs demonstrated significant antibacterial activity, inhibiting the growth of E. coli and B. subtilis. The outcomes of this study underscore the achievement in nanotechnology through the environmentally friendly synthesis of gold nanoparticles using aloe vera. This innovative combination of gold nanoparticles and aloe vera not only leverages the exceptional properties of nanomaterials but also integrates the inherent therapeutic qualities of aloe vera, enhancing its efficacy in antibacterial applications. Positioned at the convergence of nanoscience and biotechnology, this research indicates a greener and more efficient approach to addressing bacterial infections in the dynamic landscape of nanomedicine.

ACKNOWLEDGMENTS

This work is funded by the Commission on Higher Education - Leading the Advancement of Knowledge in Agriculture and Sciences (CHED-LAKAS) Program. We would also like to acknowledge the Center for Sustainable Polymers (CSP), Bio-Process Research Laboratory (BPRL) Premier Research Institute in Science and Mathematics (PRISM) of Mindanao State University – Iligan Institute of Technology (MSU-IIT), and Integrated Electron Microscope Laboratory, Central Instrumentation Facility – De La Salle University – Laguna for the equipment used in the characterization. R.L. would also like to thank the Department of Science and Technology through the Accelerated Science and Technology Human Resource Development Program (DOST-ASTHRDP) for the scholarship grant.

CONFLICTS OF INTEREST

There are no conflicts to declare.

REFERENCES

1. Khan, I.; Saeed, K.; Khan, I.; *Arab. J. Chem*. **2019**, 12,(7), 908–931.
2. Baig, N.; Kammakakam, I.; Falath, W.; *Mater. Adv*. **2021**, 2 (6), 1821–1871.
3. Altammar, K. A. *Front. Microbiol.* **2023**, 14, 1155622.
4. Yaqoob, S. B.; Adnan, R.; Rameez Khan, R. M.; Rashid, M.; *Front. Chem*. **2020**, *8*, 376.
5. Saleh, H. M.; Hassan, A. I.; *Sustainability*, **2023**, 15, 10891.
6. Yaraki, M. T.; Zahed Nasab, S.; Zare, I.; Dahri, M.; Moein Sadeghi, M.; Koohi, M.; Tan, Y. N; *Ind. Eng. Chem. Res.* **2022**, 61 (22), 7547–7593.
7. Mobed, A.; Hasanzadeh, M.; Seidi, F.; *RSC Adv.* **2021**, 11 (55), 34688–34698.
8. Shamaila, S.; Zafar, N.; Riaz, S.; Sharif, R.; Nazir, J.; Naseem, S.; *Nanomaterials*, **2016**, 6 (4), 71.
9. Luo, L.; Huang, W.; Zhang, J.; Yu, Y.; Sun, T.; *ACS Appl. Nano Mater*. **2024**, 7 (3), 2529–2545.
10. Franco, D.; Calabrese, G.; Guglielmino, S. P. P.; Conoci, S.; *Microorganisms*, **2022**, 10 (9), 1778.
11. Slavin, Y. N.; Asnis, J.; Häfeli, U. O.; Bach, H.; *J. Nanobiotechnology*, **2017**, 15 (1), 65.
12. Gu, X.; Xu, Z.; Gu, L.; Xu, H.; Han, F.; Chen, B.; Pan, X.; *Environ. Chem. Lett.*, **2021**, 19 (1), 167–187.
13. Penders, J.; Stolzoff, M.; Hickey, D. J.; Andersson, M.; Webster, T. J.; *Int. J. Nanomedicine*, **2017**, 12, 2457–2468.
14. Cui, Y.; Zhao, Y.; Tian, Y.; Zhang, W.; Lü, X.; Jiang, X.; *Biomaterials*, **2012**, 33 (7), 2327–2333.
15. Zhou, M.; Wang, B.; Rozynek, Z.; Xie, Z.; Fossum, J. O.; Yu, X.; Raaen, S.; *Nanotechnology*, **2009**, 20 (50), 505606.
16. Ielo, I.; Rando, G.; Giacobello, F.; Sfameni, S.; Castellano, A.; Galletta, M.; Drommi, D.; Rosace, G.; Plutino, M. R.; *Molecules*, **2021**, 26 (19), 5823.
17. Rahimi, H.R.; Doostmohammadi, M.; Stoytcheva, M., Zlatev, R., Eds.; *IntechOpen*, **2020**.
18. Kunjiappan, S.; Chowdhury, R.; Bhattacharjee, C.; *Front. Mater. Sci.* **2014**, 8 (2), 123–135.
19. Ahmad, T.; Bustam, M. A.; Irfan, M.; Moniruzzaman, M.; Asghar, H. M. A.; Bhattacharjee, S.; *Biotechnol. Appl. Biochem*. **2019**, 66 (4), 698–708.
20. Hosny, M.; Eltaweil, A. S.; Mostafa, M.; El-Badry, Y. A.; Hussein, E. E.; Omer, A. M.; Fawzy, M.; *ACS Omega*, **2022**, 7 (3), 3121–3133.
21. Kumar, V.; Yadav, S. K.; *J. Chem. Technol. Biotechnol.* **2009**, 84(2), 151–157.
22. Ahmed, S.; Annu; Ikram, S.; Yudha S. S.; *J. Photochem. Photobiol. B*, **2016**, 161, 141–153.
23. Zuhrotun, A.; Oktaviani, D. J.; Hasanah, A. N.; *Molecules* **2023**, 28 (7), 3240.
24. Hamelian, M.; Hemmati, S.; Varmira, K.; Veisi, H.; *J. Taiwan Inst. Chem. Eng.* **2018**, 93, 21–30.
25. Thakare, N. R.; Ingole, P. G.; Hazarika, S.; *ACS Omega*, **2023**, 8(48), 45301–45312.
26. Dudhane, A. A.; Waghmode, S. R.; Dama, L. B.; Sonawane, A.; Katariya, S.; *Int. J. Nanosci. Nanotech*. 2019, 15 (2), 75-82
27. Basavegowda, N.; Dhanya Kumar, G.; Tyliszczak, B.; Wzorek, Z.; Sobczak-Kupiec, A.; *Ann. Agric. Environ. Med.* **2015**, 22 (1), 84–89.
28. Aljabali, A.; Akkam, Y.; Al Zoubi, M.; Al-Batayneh, K.; Al-Trad, B.; Abo Alrob, O.; Alkilany, A.; Benamara, M.; Evans, D.; *Nanomaterials*, **2018**, 8 (3), 174.
29. Poojary, M. M.; Passamonti, P.; Adhikari, A. V.; *BioNanoScience*, **2016**, 6 (2), 110–120.
30. Kumar, P. V.; Kala, S. M. J.; Prakash, K. S.; *Rasayan J. Chem*. **2018**, 11 (4), 1544–1551.
31. Alshahrani, M. Y.; Rafi, Z.; Alabdallah, N. M.; Shoaib, A.; Ahmad, I.; Asiri, M.; Zaman, G. S.; Wahab, S.; Saeed, M.; Khan, S.; A *Plants*, **2021**, 10 (11), 2278.
32. Moosavy, M.-H.; De La Guardia, M.; Mokhtarzadeh, A.; Khatibi, S. A.; Hosseinzadeh, N.; Hajipour, N.; *Sci. Rep.*, **2023**, 13 (1), 7230.
33. Veena, S.; Devasena, T.; Sathak, S. S. M.; Yasasve, M.; Vishal, L. A.; *J. Clust. Sci.*, **2019**, 30 (6), 1591–1597.
34. Dauthal, P.; Mukhopadhyay, M.; *Ind. Eng. Chem. Res.*, **2016**, 55 (36), 9557–9577.
35. Majumder, R.; Das, C. K.; Mandal, M.; *Pharmacol. Res.*, **2019**, 148, 104416.
36. Athiban, P.; Borthakur, B.; Ganesan, S.; Swathika, B.; *J. Conserv. Dent.*, **2012**, 15 (3), 246.
37. Carac, A.; Boscencu, R.; Patriche, S.; Dinica, R. M.; Carac, G.; Gird, C. E.; *Revista de Chimie*, **2016**, 67 (4), 654-658.
38. Tippayawat, P.; Phromviyo, N.; Boueroy, P.; Chompoosor, A.; *PeerJ*, **2016**, 4, e2589.
39. Kumar, P. P. N. V.; Shameem, U.; Kollu, P.; Kalyani, R. L.; Pammi, S. V. N.; *BioNanoScience*, **2015**, 5 (3), 135–139.
40. Chandran, S. P.; Chaudhary, M.; Pasricha, R.; Ahmad, A.; Sastry, M.; *Biotechnol. Prog.* **2006**, 22 (2), 577–583.
41. Muralikrishna, T.; Pattanayak, M.; Nayak, P. L.; *World J. Nano Sci. Technol.* **2014**, 3(2), 45-51.
42. Philip, D.; *Acta. A. Mol. Biomol. Spectrosc.* **2008**, 71 (1), 80–85.
43. Aljarrah, M. T.; Alboull, A. M.; Alharahsheh, M. S.; Ashraf, A.; Khandakar, A.; *Molecules*, **2022**, 27 (24), 8651.
44. Mustafa, D. E.; Yang, T.; Xuan, Z.; Chen, S.; Tu, H.; Zhang, A.; *Plasmonics*, **2010**, 5 (3), 221–231.
45. Dahan, K. A.; Li, Y.; Xu, J.; Kan, C.; *Phys. Chem. Chem. Phys.* **2023**, 25 (28), 18545–18576.
46. Thanh, N. T. K.; Maclean, N.; Mahiddine, S.; *Chem. Rev.* **2014**, 114 (15), 7610–7630.
47. Maguire, C. M.; Rösslein, M.; Wick, P.; Prina-Mello, A.; *Sci. Technol. Adv. Mater.* **2018**, 19 (1), 732–745.
48. Hiemenz, P. C.; Rajagopalan, R.; Principles of Colloid and Surface Chemistry, 3rd ed., rev.expanded.; Marcel Dekker: New York, **1997**.
49. Ravi, S.; Kabilar, P.; Velmurugan, S.; Kumar, R. A.; Gayathiri, M.; *Journal of Experimental Sciences*, **2011**, 2, 10-13.
50. Ray, A.; Ghosh, S.; *Mater. Today Proc.* **2018**, 5 (10), 22245–22253.
51. Timoszyk, A.; Grochowalska, R.; *Pharmaceutics*, **2022**, 14 (12), 2599.
52. Huang, X.; Devi, S.; Bordiga, M.; Brennan, C. S.; Xu, B.; *Int. J. Food Sci. Technol.* **2023**, 58 (4), 1673–1694.
53. Bindhu, M. R.; Umadevi, M.; *Mater. Lett.* **2014**, 120, 122–125.
54. Ali, K.; Dwivedi, S.; Azam, A.; Saquib, Q.; Al-Said, M. S.; Alkhedhairy, A. A.; Musarrat, J.; *J. Colloid Interface Sci.* **2016**, 472, 145–156.
55. Breijyeh, Z.; Jubeh, B.; Karaman, R.; *Molecules*, **2020**, 25 (6), 1340.
56. Hameed, S.; Wang, Y.; Zhao, L.; Xie, L.; Ying, Y.; *Mater. Sci. Eng. C*, **2020**, 108, 110338.
57. Contini, C.; Hindley, J. W.; Macdonald, T. J.; Barritt, J. D.; Ces, O.; Quirke, N.; *Commun. Chem.*, **2020**, 3 (1), 130.
58. Osonga, F. J.; Akgul, A.; Yazgan, I.; Akgul, A.; Eshun, G. B.; Sakhaee, L.; Sadik, O. A.; *Molecules*, **2020**, 25 (11), 2682.
59. Draviana, H. T.; Fitriannisa, I.; Khafid, M.; Krisnawati, D. I.; Widodo; Lai, C. H.; Fan, Y. J.; Kuo, T. R.; *J. Nanobiotechnology*, **2023**, 21 (1), 428.
60. Dikshit, P.; Kumar, J.; Das, A.; Sadhu, S.; Sharma, S.; Singh, S.; Gupta, P.; Kim, B.; *Catalysts*, **2021**, 11 (8), 902.

Advanced Materials Letters
https://aml.iaamonline.org

GRAPHICAL ABSTRACT

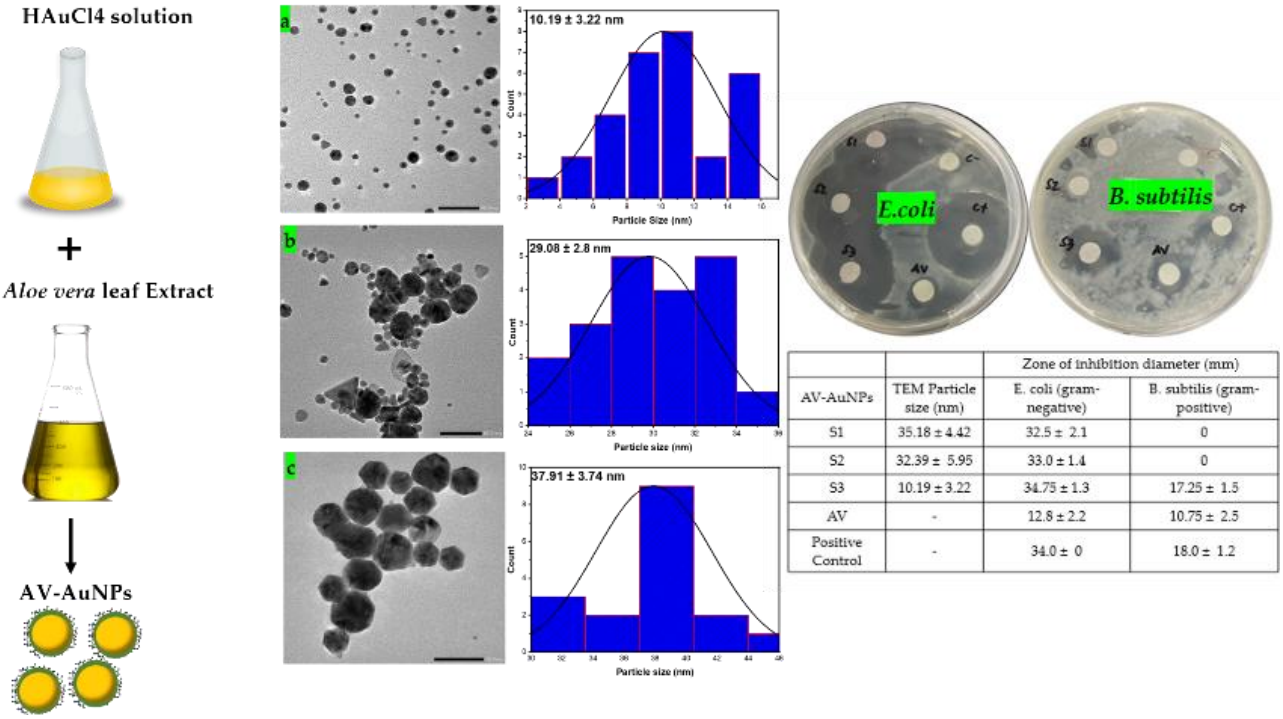

AV-AuNPs	TEM Particle size (nm)	Zone of inhibition diameter (mm)	
		E. coli (gram-negative)	B. subtilis (gram-positive)
S1	35.18 ± 4.42	32.5 ± 2.1	0
S2	32.39 ± 5.95	33.0 ± 1.4	0
S3	10.19 ± 3.22	34.75 ± 1.3	17.25 ± 1.5
AV	-	12.8 ± 2.2	10.75 ± 2.5
Positive Control	-	34.0 ± 0	18.0 ± 1.2